Proceedings of the
44th IEEE Conference on Decision and Control, and
the European Control Conference 2005
Seville, Spain, December 12-15, 2005

A Control-Oriented Analysis of Bio-inspired Visuomotor Convergence[1]

J. Sean Humbert[†]
Richard M. Murray[*] and Michael H. Dickinson[*]

***Abstract*— Insects exhibit incredibly robust closed loop flight dynamics in the face of uncertainties. A fundamental principle contributing to this unparalleled behavior is rapid processing and convergence of visual sensory information to flight motor commands via spatial wide-field integration, accomplished by retinal motion pattern sensitive interneurons (LPTCs) in the lobula plate portion of the visual ganglia. Within a control-theoretic framework, models for spatially continuous retinal image flow and wide-field integration processing are developed, establishing the connection between image flow kernels (retinal motion pattern sensitivities) and the feedback terms they represent. It is shown that these outputs are sufficient to stabilize speed regulation and terrain following tasks. Hence, extraction of global retinal motion cues through computationally efficient wide-field integration processing provides a novel and promising methodology for utilizing visual sensory information in autonomous robotic navigation and flight control applications.**

I. INTRODUCTION

Prevalent in many natural sensory systems is the phenomenon of sensorimotor convergence, wherein signals from arrays of spatially distributed and differentially tuned sensors converge in vast numbers onto motor neurons responsible for controlling locomotive behavior. A prime example occurs in the processing of retinal image pattern movement (optic flow) by the visuomotor systems of insects (Figure 2A). Insect visual systems encode optic flow by combining motion estimates from arrays of local movement detectors in a way that preserves the spatial layout of the retina [1]. This spatially preserved motion information is parsed by wide-field motion sensitive interneurons in the lobula plate section of the visual ganglia (called tangential cells, or LPTCs for short). The output of these neurons is communicated via decending neurons to the motor control centers, creating a sensory processing front end that spatially integrates the optic flow [2]. This visuomotor convergence technique, spatial wide-field integration, is presumed to be used by insects to extract behaviorally relevant information from optic flow patterns to modulate the kinematics of flight [3].

Since optic flow was first recognized as a critical source of information [4], there has been considerable interest in adapting this type of sensory system for bio-inspired autonomous navigation. One concept that has recently received a significant amount of attention is that of the biological *matched filter* [5], where the neural images formed from sensory inputs are compared with pre-determined templates, presumably to assist in determination of behavioral responses [6]. As receptive field structure of particular tangential interneurons (VS cells [7] and HS cells [8]) have revealed similarites to the equivalent projected velocity fields for certain cases of rotary self motion, it has been postulated [9] that LPTCs extract particular types of self-motion from optic flow fields.

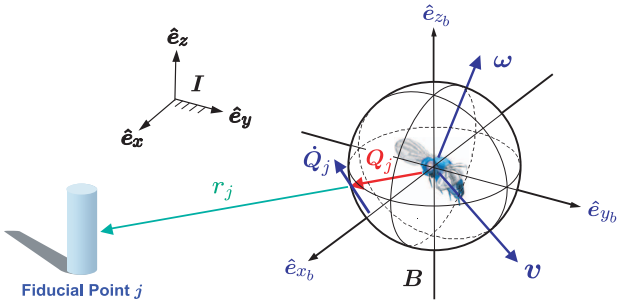

Fig. 1. Motion Parallax Field Definitions

In this paper we propose a more general functional role for wide-field sensitive neurons in navigation and flight control as well as a novel methodology for utilizing optic flow sensory information in robotic applications. We show how the spatial harmonics of planar optic flow, extracted with motion-pattern sensitive kernels representing LPTCs (Figure 2B), correspond to feedback terms which can be used to stabilize navigational tasks. Section II develops the equations that govern spherical motion parallax fields of three dimensional environments. A model for wide-field integration of planar retinal image flow is presented in Section III, and the connection between image flow kernels and the output feedback terms they represent is established. In Section IV an output feedback methodology based on wide-field integration sensory information is presented along with simulations demonstrating speed regulation and terrain following behavior for wheeled robot dynamics.

II. A SPATIALLY CONTINUOUS MODEL OF OPTIC FLOW

The basic set of equations that specify a general spatially discrete optic flow field for a spherical retinal surface geometry and an environment composed of $j = 1 \dots N$ rigid fiducial points (Figure 1) was developed in [10]:

$$\dot{\boldsymbol{Q}}_j \;=\; -\boldsymbol{\omega} \times \boldsymbol{Q}_j - \frac{1}{r_j}\left[\boldsymbol{v} - \langle \boldsymbol{v}, \boldsymbol{Q}_j \rangle \boldsymbol{Q}_j\right]. \qquad (1)$$

A fiducial point j is located with respect to the vantage point, i.e., the origin of the rigidly attached body frame coordinate system $\boldsymbol{B} = (\hat{\boldsymbol{e}}_{x_b}, \hat{\boldsymbol{e}}_{y_b}, \hat{\boldsymbol{e}}_{z_b})$, by a vector $\boldsymbol{r}_j \in \mathbb{R}^3$

[1] Partial support for this work was provided by AFOSR under grant F30602-01-2-0558 and ARO under grant DAAD19-03-D-0004

[†] Department of Aerospace Engineering, University of Maryland, College Park, MD 20742, *humbert@umd.edu*

[*] Engineering and Applied Science, Caltech, Pasadena, CA 91125

0-7803-9568-9/05/$20.00 ©2005 IEEE

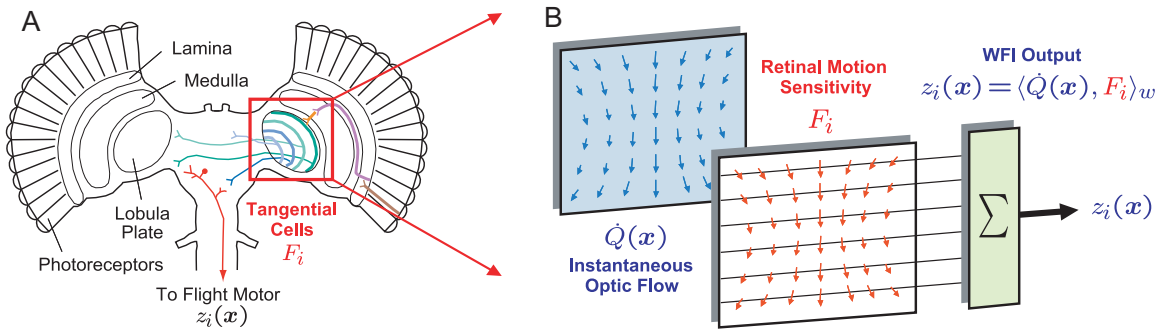

Fig. 2. (A) Visuomotor system of insects. Wide-field retinal motion sensitive interneurons (tangential cells) parse spatially-preserved visual information and transmit it to motor control centers. (B) WFI processing model. Spatial modes of optic flow are extracted by retinal motion sensitivity kernels.

with magnitude $r_j = \|\boldsymbol{r}_j\|$ along marker $\boldsymbol{Q}_j = \boldsymbol{r}_j / r_j$. In this formulation, the motion parallax $\dot{\boldsymbol{Q}}_j = \dot{\boldsymbol{Q}}_{\boldsymbol{\omega},j} + \dot{\boldsymbol{Q}}_{\boldsymbol{v},j}$ is defined as the time derivative of the marker $\boldsymbol{Q}_j \in S^2$, which has contributions from both the angular and linear velocities $\boldsymbol{\omega}, \boldsymbol{v} \in \mathbb{R}^3$ of the body frame $\boldsymbol{B}$ with respect to an inertial frame $\boldsymbol{I} = (\hat{\boldsymbol{e}}_x, \hat{\boldsymbol{e}}_y, \hat{\boldsymbol{e}}_z)$. The rotational contribution, $\dot{\boldsymbol{Q}}_{\boldsymbol{\omega},j} = -\boldsymbol{\omega} \times \boldsymbol{Q}_j$, produces a velocity field independent of the distances to objects in the environment. The translational contribution, $\dot{\boldsymbol{Q}}_{\boldsymbol{v},j} = \frac{1}{r_j}\left[\boldsymbol{v} - \langle \boldsymbol{v}, \boldsymbol{Q}_j \rangle \boldsymbol{Q}_j\right]$, is the relative linear velocity of the fiducial point, scaled inversely by the distance, with the radial component removed. Collectively, the set of markers and motion parallax vectors $\{\boldsymbol{Q}_j, \dot{\boldsymbol{Q}}_j, j = 1 \ldots N\}$ compose a general spatially discrete optic flow field.

For a continuous representation of the spatial distribution of the environment, the instantaneous set of distances to the fiducial points $\{r_i, i = 1 \ldots N\}$ becomes a function of the azimuth and elevation angles $r(\gamma, \beta) : [0, 2\pi] \times [-\frac{\pi}{2}, \frac{\pi}{2}] \mapsto (0, \infty)$. Implicit to this definition, r also depends on the particular environment as well as the vantage point configuration $\mathbf{q}(t)$, i.e., the position and orientation within that environment. We expect this function to take on values from $(0, \infty)$ and contain discontinuities, especially in a cluttered object field. By explicitly disallowing contact $r(\gamma, \beta, \mathbf{q}) = 0$, we ensure that the reciprocal, defined as the *nearness*,

$$\mu(\gamma, \beta, \mathbf{q}) \quad = \quad \frac{1}{r(\gamma, \beta, \mathbf{q})}\,, \tag{2}$$

is a bounded, piecewise continuous function with a finite (countable) number of discontinuities and at each instant in time is restricted to the space of square integrable functions $L_2\left([0, 2\pi] \times [-\frac{\pi}{2}, \frac{\pi}{2}]\right)$

A. Rotational Optic Flow

We would like to express the optic flow in terms of quanities that are useful for feedback control; hence we define the roll, pitch, and yaw rates as the projections of the body frame angular velocity $\boldsymbol{\omega}$ onto the unit directions for $\boldsymbol{B}$,

$$\boldsymbol{\omega} \quad = \quad \dot{\psi}\, \hat{\boldsymbol{e}}_{x_b} + \dot{\phi}\, \hat{\boldsymbol{e}}_{y_b} + \dot{\theta}\, \hat{\boldsymbol{e}}_{z_b}. \tag{3}$$

For this spatially continuous formulation, we express a general point on the sphere $\boldsymbol{Q} \in S^2$ in terms of the azimuth γ and elevation β angles in $\boldsymbol{B}$ (Figure 3A):

$$\boldsymbol{Q}(\gamma, \beta) = \cos\gamma \cos\beta\, \hat{\boldsymbol{e}}_{x_b} + \sin\gamma \cos\beta\, \hat{\boldsymbol{e}}_{y_b} + \sin\beta\, \hat{\boldsymbol{e}}_{z_b}, \tag{4}$$

Now considered as an operator $\hat{\boldsymbol{Q}}_{\boldsymbol{\omega}} : \mathbb{R}^3 \mapsto \mathbb{R}^3$, the map $\boldsymbol{\omega} \mapsto -\boldsymbol{\omega} \times \boldsymbol{Q}$ is linear and has a skew-symmetric matrix representation

$$\hat{\boldsymbol{Q}} \quad = \quad \begin{pmatrix} 0 & -\sin\beta & \sin\gamma\cos\beta \\ \sin\beta & 0 & -\cos\gamma\cos\beta \\ -\sin\gamma\cos\beta & \cos\gamma\cos\beta & 0 \end{pmatrix}.$$

Hence, the rotational optic flow field in $\boldsymbol{B}$ coordinates is given by

$$\dot{\boldsymbol{Q}}_{\boldsymbol{\omega}} \quad = \quad \hat{\boldsymbol{Q}}\boldsymbol{\omega}. \tag{5}$$

B. Translational Optic Flow

As in the rotational contribution, we define the forward, lateral, and vertical velocities as projections of the body frame linear velocity $\boldsymbol{v}$ onto the unit directions for $\boldsymbol{B}$:

$$\boldsymbol{v} \quad = \quad \dot{x}_b\, \hat{\boldsymbol{e}}_{x_b} + \dot{y}_b\, \hat{\boldsymbol{e}}_{y_b} + \dot{z}_b\, \hat{\boldsymbol{e}}_{z_b}. \tag{6}$$

Using the definition (4), the operator $\boldsymbol{v} \mapsto \boldsymbol{v} - \langle \boldsymbol{v}, \boldsymbol{Q} \rangle \boldsymbol{Q}$ can be written compactly as

$$\left(I - \boldsymbol{Q}\boldsymbol{Q}^T\right) = \begin{pmatrix} 1 - \mathrm{c}^2\gamma\mathrm{c}^2\beta & -\mathrm{c}^2\beta\mathrm{s}\gamma\mathrm{c}\gamma & -\mathrm{c}\gamma\mathrm{s}\beta\mathrm{c}\beta \\ -\mathrm{c}\gamma\mathrm{s}\gamma\mathrm{c}^2\beta & 1 - \mathrm{s}^2\gamma\mathrm{c}^2\beta & -\mathrm{s}\gamma\mathrm{s}\beta\mathrm{c}\beta \\ -\mathrm{c}\gamma\mathrm{s}\beta\mathrm{c}\beta & -\mathrm{s}\gamma\mathrm{s}\beta\mathrm{c}\beta & 1 - \mathrm{s}^2\beta \end{pmatrix},$$

where $\mathrm{s}\gamma = \sin\gamma$ and $\mathrm{c}\beta = \cos\beta$. To obtain the translational optic flow field in $\boldsymbol{B}$ coordinates, we scale by the nearness function (2):

$$\dot{\boldsymbol{Q}}_{\boldsymbol{v}} \quad = \quad \mu\left(I - \boldsymbol{Q}\boldsymbol{Q}^T\right)\boldsymbol{v}. \tag{7}$$

C. Spherical Coordinates

The action of (7) is to extract the radial component from the velocity field of stationary objects relative to the moving body frame $\boldsymbol{B}$. Therefore, for an arbitrary point $\boldsymbol{Q}(\gamma, \beta) \in S^2$ on a spherical sensor or retina, the resulting translational optic flow vector at that location is the projection of the relative velocity of the point on the nearest object along direction $\boldsymbol{Q}$ into the tangent space $T_{\boldsymbol{Q}}S^2$ at the point $\boldsymbol{Q}$, i.e., $\left(I - \boldsymbol{Q}\boldsymbol{Q}^T\right) : \mathbb{R}^3 \mapsto TS^2$. The same result may be concluded regarding the action of (5): $\hat{\boldsymbol{Q}} : \mathbb{R}^3 \mapsto TS^2$.

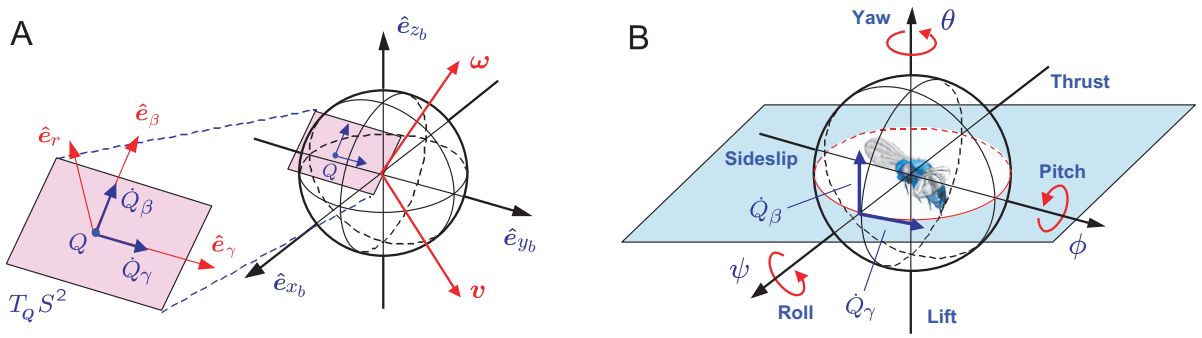

Fig. 3. Spherical retinal geometry. (A) Spherical coordinate definitions (B) Spherical optic flow components $\dot{Q}_\gamma$ and $\dot{Q}_\beta$ for planar applications.

Therefore, it makes sense to put (5) and (7) into spherical coordinates, by applying the transformation from rectangular coordinates

$$R = \begin{pmatrix} \cos\gamma\cos\beta & \sin\gamma\cos\beta & \sin\beta \\ -\sin\gamma & \cos\gamma & 0 \\ -\cos\gamma\sin\beta & -\sin\gamma\sin\beta & \cos\beta \end{pmatrix}.$$

The resulting spherical coordinate representation $\dot{\boldsymbol{Q}} = \dot{Q}_\gamma\,\hat{\boldsymbol{e}}_\gamma + \dot{Q}_\beta\,\hat{\boldsymbol{e}}_\beta$ is given by

$$\dot{\boldsymbol{Q}} = A\boldsymbol{\omega} + \mu B\boldsymbol{v}. \tag{8}$$

The matricies $A(\gamma,\beta) = R\hat{\boldsymbol{Q}}$ and $B(\gamma,\beta) = -R\left(I - \boldsymbol{Q}\boldsymbol{Q}^T\right)$, reflecting the spherical retina geometry, are given by

$$A(\gamma,\beta) = \begin{pmatrix} \sin\beta\cos\gamma & \sin\beta\sin\gamma & -\cos\beta \\ \sin\gamma & \cos\gamma & 0 \end{pmatrix}$$

$$B(\gamma,\beta) = \begin{pmatrix} -\sin\gamma & \cos\gamma & 0 \\ -\sin\beta\cos\gamma & -\sin\beta\sin\gamma & \cos\beta \end{pmatrix}.$$

It is further assumed that the kinematics $\dot{\mathbf{q}} = (\boldsymbol{v},\boldsymbol{\omega})$ of the body frame $\boldsymbol{B}$ are bounded, piecewise-continuous functions of time; hence the instantaneous optic flow components $\dot{Q}_\gamma$ and $\dot{Q}_\beta$, given by (8), are restricted to the function space $L_2\left([0,2\pi]\times[-\frac{\pi}{2},\frac{\pi}{2}]\right)$.

D. Planar Applications

The tangential and normal optic flow components $\dot{Q}_\gamma$ and $\dot{Q}_\beta$ for the circle defined by the intersection of S^2 and the plane $\beta = 0$ (Figure 3B) are given by

$$\dot{Q}_\gamma = -\dot{\theta} + \mu(\gamma,0,\mathbf{q})\,(\dot{x}_b\sin\gamma - \dot{y}_b\cos\gamma) \tag{9}$$

$$\dot{Q}_\beta = -\dot{\psi}\sin\gamma + \dot{\phi}\cos\gamma - \mu(\gamma,0,\mathbf{q})\,\dot{z}_b \tag{10}$$

For motion restricted to the plane $\beta = 0$, we define the vehicle configuration $\mathbf{q} = (x,y,\theta)$ and velocity $\dot{\mathbf{q}} = (\dot{x}_b,\dot{y}_b,\dot{\theta})$ with respect to an inertial (static) environment. Under these conditions, the normal component $\dot{Q}_\beta$ is zero, and the tangential component $\dot{Q}_\gamma$ becomes a 2π-periodic function of the vehicle-referred viewing angle γ. Clearly for fixed t, $\mu(\gamma,0,\mathbf{q}) \in L_2[0,2\pi]$ and therefore $\dot{Q}_\gamma \in L_2[0,2\pi]$. For notational convenience we will refer to the planar nearness function for the environment of interest as $\mu(\gamma,\mathbf{q})$, noting the dependence on components of the configuration of the vehicle. In addition we will drop the γ subscript and refer to the tangential optic flow component as $\dot{Q}(\gamma,\mathbf{q},\dot{\mathbf{q}})$, noting the dependence on the vehicle's configuration and velocity:

$$\dot{Q}(\gamma,\mathbf{q},\dot{\mathbf{q}}) = -\dot{\theta} + \mu(\gamma,\mathbf{q})\,(\dot{x}_b\sin\gamma - \dot{y}_b\cos\gamma)\,. \tag{11}$$

III. A Model for Wide-Field Integration Processing of Ideal Planar Optic Flow

For this treatment we will represent the lobula plate tangential cells (or ispi- and contralateral pairs as may be appropriate) by a general weight $F_i(\gamma) \in L_2[0,2\pi]$, which models their sensitivity to retinal motion patterns (Figure 2A). Weights $F_i(\gamma)$ are essentially a spatially distributed set static gains that are applied to the output at the corresponding local motion detectors at retinal azumuthal positions γ (Figure 2B). With the analysis presented here, we are interested in characterizing the available information relevant for use in closed loop feedback. We expect these retinal motion pattern sensitivities to be piecewise continuous and square-integrable; hence the restriction to the function space $L_2[0,2\pi]$. For this analysis we will also assume that optic flow estimation processing (photoreceptors and local motion detectors) have negligible dynamics, that is, wide-field spatial integration (henceforth WFI) can be modeled in entirety by a transformation W, representing a spatial inner product over the circle S^1 with the optic flow kernel (11) which acts on elements $F_i(\gamma)$ to produce a sensor output signal $z_i(\mathbf{q},\dot{\mathbf{q}})$, hence $W : F_i \in L_2[0,2\pi] \mapsto z_i \in \mathbb{R}$. The transformation W defined by $z_i = WF_i$ can be represented as a linear functional using the inner product structure available on $L_2[0,2\pi]$:

$$z_i(\mathbf{q},\dot{\mathbf{q}}) = \langle\dot{Q},F_i\rangle_w = \frac{1}{\pi}\int_0^{2\pi}\dot{Q}(\gamma,\mathbf{q},\dot{\mathbf{q}})\cdot F_i(\gamma)\,d\gamma. \tag{12}$$

The inner product (12) has been defined with a factor of $1/\pi$ to be compatible with the typical Fourier harmonic component definition so that later notation is simplified.

A. Characterization of WFI Sensory Outputs

We are interested in characterizing the set of all possible sensory outputs available within this model and their dependency on vehicle motion and spatial distribution of objects in the environment. Since $L_2[0,2\pi]$ is a separable Hilbert space, a countably infinite orthonormal basis $\{\phi_n(\gamma)\}$ exists. For

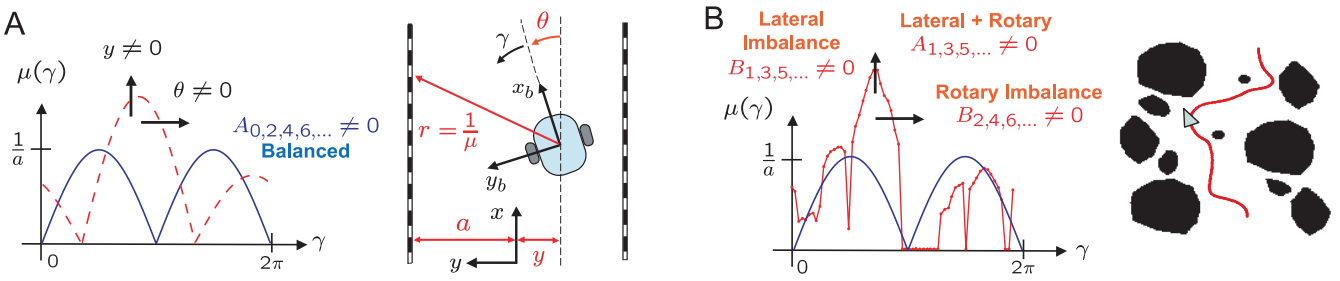

Fig. 4. Connections between WFI outputs and μ. (A) Planar tunnel geometry and lateral/rotational perturbations of μ (B) μ-shaping in environments with higher order spatial structure

every instant in time, the optic flow (11) resides in $L_2[0, 2\pi]$; therefore, we are guaranteed a unique generalized Fourier series expansion $\dot{Q} = \sum_n c_n \, \phi_n$, where $c_n = \langle \dot{Q}, \phi_n \rangle_w$. For the orthonormal basis

$$\Phi \;=\; \{1/\sqrt{2}\} \cup \{\cos n\gamma : n \in \mathbb{Z}^+\} \cup \{\sin n\gamma : n \in \mathbb{Z}^+\},$$

the expansion becomes

$$\dot{Q} \;=\; \frac{a_0}{2} + \sum_{n=1}^{\infty} a_n \cos n\gamma + \sum_{n=1}^{\infty} b_n \sin n\gamma,$$

where the Fourier coefficients of the optic flow, which are functions of the configuration and velocity, are defined as

$$\begin{aligned} a_0(\mathbf{q}, \dot{\mathbf{q}}) &= \langle \dot{Q}, 1/\sqrt{2} \rangle_w &&= \tfrac{1}{\pi} \textstyle\int_0^{2\pi} \dot{Q}(\gamma, \mathbf{q}, \dot{\mathbf{q}})/\sqrt{2} \; d\gamma \\ a_n(\mathbf{q}, \dot{\mathbf{q}}) &= \langle \dot{Q}, \cos n\gamma \rangle_w &&= \tfrac{1}{\pi} \textstyle\int_0^{2\pi} \dot{Q}(\gamma, \mathbf{q}, \dot{\mathbf{q}}) \cdot \cos n\gamma \; d\gamma \\ b_n(\mathbf{q}, \dot{\mathbf{q}}) &= \langle \dot{Q}, \sin n\gamma \rangle_w &&= \tfrac{1}{\pi} \textstyle\int_0^{2\pi} \dot{Q}(\gamma, \mathbf{q}, \dot{\mathbf{q}}) \cdot \sin n\gamma \; d\gamma. \end{aligned}$$

With some manipulations, we can re-write these expressions in terms of the vehicle velocity $\dot{\mathbf{q}} = (\dot{x}_b, \dot{y}_b, \dot{\theta})$ and the spatial harmonics $\{A_0(\mathbf{q}), A_k(\mathbf{q}), B_k(\mathbf{q}) : k \in \mathbb{Z}^+\}$ of the nearness function $\mu(\gamma, \mathbf{q})$:

$$\begin{aligned} a_0 &= (-\dot{\theta} + \dot{x}_b B_1 - \dot{y}_b A_1)/\sqrt{2} \\ a_n &= \frac{\dot{x}_b}{2}(-B_{n-1} + B_{n+1}) - \frac{\dot{y}_b}{2}(A_{n-1} + A_{n+1}) \\ b_n &= \frac{\dot{x}_b}{2}(A_{n-1} - A_{n+1}) - \frac{\dot{y}_b}{2}(B_{n-1} + B_{n+1}), \end{aligned} \tag{13}$$

where the nearness function has been expanded in the orthonormal basis Φ:

$$\mu \;=\; \frac{A_0}{2} + \sum_{k=1}^{\infty} A_k \cos n\gamma + \sum_{k=1}^{\infty} B_k \sin n\gamma,$$

and whose configuration-dependent Fourier series coefficients are defined as

$$\begin{aligned} A_0(\mathbf{q}) &= \langle \mu, 1/\sqrt{2} \rangle_w &&= \tfrac{1}{\pi} \textstyle\int_0^{2\pi} \mu(\gamma, \mathbf{q})/\sqrt{2} \; d\gamma \\ A_k(\mathbf{q}) &= \langle \mu, \cos k\gamma \rangle_w &&= \tfrac{1}{\pi} \textstyle\int_0^{2\pi} \mu(\gamma, \mathbf{q}) \cdot \cos k\gamma \; d\gamma \\ B_k(\mathbf{q}) &= \langle \mu, \sin k\gamma \rangle_w &&= \tfrac{1}{\pi} \textstyle\int_0^{2\pi} \mu(\gamma, \mathbf{q}) \cdot \sin k\gamma \; d\gamma. \end{aligned}$$

Now, under the interpretation

$$W\Phi \;=\; \{a_0\} \cup \{a_n : n \in \mathbb{Z}^+\} \cup \{b_n : n \in \mathbb{Z}^+\},$$

the equations (13) define the action of the linear transformation $W : L_2[0, 2\pi] \mapsto \mathbb{R}$ on a basis Φ for the domain, and as such uniquely characterize the set of all possible wide-field integration sensory outputs.

TABLE I
INTERPRETATION OF μ SPATIAL FOURIER HARMONICS A_k,B_k

Mode	Balanced	General Tunnel	Imbalance
A_0	$\frac{2}{a\pi}$	$\frac{2a}{\pi(a^2-y^2)}$	-
A_1	0	$\frac{y \sin\theta}{(a^2-y^2)}$	Lateral + Rotary
B_1	0	$\frac{y \cos\theta}{(a^2-y^2)}$	Lateral
$A_{2,4,6,\ldots}$	$-\frac{4}{a\pi(k^2-1)}$	$-\frac{4a \cos k\theta}{\pi(a^2-y^2)(k^2-1)}$	-
$B_{2,4,6,\ldots}$	0	$-\frac{4a \sin k\theta}{\pi(a^2-y^2)(k^2-1)}$	Rotary
$A_{3,5,7,\ldots}$	0	0	Lateral + Rotary
$B_{3,5,7,\ldots}$	0	0	Lateral

B. Interpretation of WFI Outputs

The relationships in (13) define how WFI outputs depend on vehicle velocity $\dot{\mathbf{q}} = (\dot{x}_b, \dot{y}_b, \dot{\theta})$ and object nearness $\mu : \{A_0, A_k, B_k : k \in \mathbb{Z}^+\}$ with respect to the vantage point configuration $\mathbf{q}$, however the intuition required to utilize them in closed loop feedback is not readily apparent. As a motivational example, we consider a planar tunnel geometry (Figure 4A), which provides a reasonable approximation to flight between two obstacles. In this case the nearness function $\mu(\gamma, \mathbf{q})$ is independent of the axial position x and can be expressed in closed form as a function of the lateral position y, body frame orientation θ, and the tunnel half-width a:

$$\mu(\gamma, \mathbf{q}) \;=\; \begin{cases} \frac{\sin(\gamma+\theta)}{a-y} & 0 \leq \gamma + \theta < \pi \\ -\frac{\sin(\gamma+\theta)}{a+y} & \pi \leq \gamma + \theta < 2\pi \end{cases}. \tag{14}$$

For a perfectly centered vehicle $(y, \theta) = (0, 0)$, (14) reduces to $|\sin\gamma| \, / a$, which has a Fourier series expansion

$$\mu(\gamma, \mathbf{q})|_{y,\theta=0} = \frac{2}{a\pi} - \sum_{k=2,4,6,\ldots}^{\infty} \frac{4}{a\pi(k^2-1)} \cos k\gamma. \tag{15}$$

Note that the expansion is composed of a DC component and even cosine harmonics $\{A_k : k = 0, 2, 4, \ldots\}$ of decreasing amplitude only. Equation (15) represents the *balanced* or *equilibrium* nearness shape (Figure 4A), as it corresponds to a position and orientation along the centerline of the tunnel. For lateral and rotary displacements, the spatial harmonics

of the perturbed nearness function are computed in Table I. From the linearizations with respect to the configuration variables $\mathbf{q} = (y, \theta)$ about about the point $\mathbf{q}_0 = (0, 0)$ it is clear that the B_1 harmonic provides an estimate of the lateral displacement while the B_2 harmonic provides an estimate of the rotary displacement.

These results can immediately be generalized to environments with more complicated spatial structure (Figure 4B). We have defined even cosine harmonics $\{A_k : k = 0, 2, 4, \ldots\}$ to represent a balanced nearness function; thus, the presence of even sine harmonics $\{B_k : k = 2, 4, \ldots\}$ indicates a rotary imbalance, odd sine harmonics $\{B_k : k = 1, 3, 5, \ldots\}$ a lateral imbalance, and odd cosine harmonics $\{A_k : k = 1, 3, 5, \ldots\}$ a coupled rotary/lateral imbalance.

IV. WFI-Based Static Output Feedback

In this section we demonstrate the utility of WFI sensory outputs (13) through coupling with planar flight dynamics via static output feedback (Figure 5). The WFI operator is

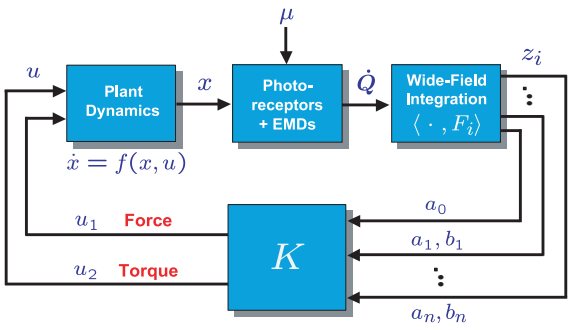

Fig. 5. Closed loop WFI output feedback

used to decompose the optic flow into spatial harmonics (13), and force and torque control inputs u_1, u_2 are computed as static combinations

$$u_i = K^a_{i0}\, a_0 + \sum_{j=1}^{n} K^a_{ij}\, a_j + K^b_{ij}\, b_j, \tag{16}$$

which correspond to motion sensitivity functions

$$F_{u_i} = K^a_{i0} + \sum_{j=1}^{n} K^a_{ij} \cos j\gamma + K^b_{ij} \sin j\gamma. \tag{17}$$

For analysis and simulation purposes we will consider rolling or wheeled vehicles of the unicycle type (Figure 4A), subject to the nonholonomic constraint $\dot{x} \sin\theta - \dot{y} \cos\theta = 0$, which enforces $\dot{y}_b = 0$. It is assumed that the two wheels providing continuous contact with the ground are driven independently, and the vehicle center of mass is located at the midpoint along the axis between them. In the inertial configuration (x, y, θ) the kinematic and dynamic equations describing the motion are

$$\begin{aligned} \dot{x} &= v \cos\theta \\ \dot{y} &= v \sin\theta \\ m\dot{v} &= (T_s + T_p)/r_w \\ J\ddot{\theta} &= r_0 (T_s - T_p)/r_w, \end{aligned} \tag{18}$$

where starboard and port wheel torques are denoted by T_s and T_p, r_0 and r_w denote the vehicle width and wheel radius, and the vehicle mass and rotational inertia are given by m and J.

A. Local Asymptotic Stability Analysis

The intent is to show feasibility of the proposed output feedback methodology, hence a linearized control design which guarentees local asymptotic stability of speed regulation and obstacle avoidance responses in the nonlinear system is discussed. It will be useful to introduce the following state and input definitions $v = \dot{x}_b$, $u_1 = (T_s + T_p)/r_w$, and $u_2 = r_0(T_s - T_p)/r_w$. Assuming small states (other than v) and control inputs, the linearized equations of motion for a centerline flight trajectory become

$$\begin{aligned} m\dot{v} &= u_1 \\ \dot{y} &= v_0\theta \\ J\ddot{\theta} &= u_2 \end{aligned} \tag{19}$$

Equation (20) shows the resulting linearization $z(\boldsymbol{x}) = z(\boldsymbol{x}_0) + \sum_i \frac{\partial z}{\partial x_i}(\boldsymbol{x}_0)\ (x_i - x_{i0})$, of outputs a_0, a_1, b_1 and a_2 for the planar tunnel with respect to the kinematic variables $\boldsymbol{x} = (v, y, \theta, \dot{\theta})$ along a reference trajectory $\boldsymbol{x}_0 = (v_0, 0, 0, 0)$, corresponding to a centerline trajectory at a constant velocity v_0.

$$\begin{pmatrix} z_{b_1} \\ z_{a_0} \\ z_{a_1} \\ z_{a_2} \end{pmatrix} = \begin{pmatrix} \frac{8}{3\pi a} & 0 & 0 & 0 \\ 0 & \frac{v_0}{\sqrt{2a^2}} & 0 & -\sqrt{2} \\ 0 & 0 & \frac{4v_0}{3\pi a} & 0 \\ 0 & -\frac{v_0}{4a^2} & 0 & 0 \end{pmatrix} \begin{pmatrix} v \\ y \\ \theta \\ \dot{\theta} \end{pmatrix} \tag{20}$$

For the forward speed regulation task, we define a reference forward velocity r and corresponding scaling factor N and close the loop by setting the thrust input

$$u_1 = K^b_{11}(Nr - b_1), \tag{21}$$

where $b_1 = \langle \dot{Q}, \sin\gamma \rangle_w$, corresponding to the motion sensitivity function

$$F_{u_1}(\gamma) = K^b_{11} \sin\gamma. \tag{22}$$

With $r = v_0$, choose $N = 8/(3\pi a)$ for zero steady-state error, and the linearized closed loop dynamics become

$$\dot{v} = -\frac{N}{m} K^b_{11}(v - v_0). \tag{23}$$

One can easily verify that with $K^b_{11} > 0$, the closed loop eigenvalue is in the open left-half plane, and therefore local stability of the nonlinear system is achieved.

A quick check of the controllability and observability matricies shows that the linearized system is completely controllable and observable about the equilibrium point $\boldsymbol{x}_0$ as long as $v_0 \neq 0$. Therefore, due to the coupling of the lateral to the rotational dynamics through the $v_0\theta$ term in (19), it is possible to accomplish stabilization of both modes via static output feedback through the torque input, taken to be

$$u_2 = K^a_{20} a_0 + K^a_{21} a_1 + K^a_{22} a_2. \tag{24}$$

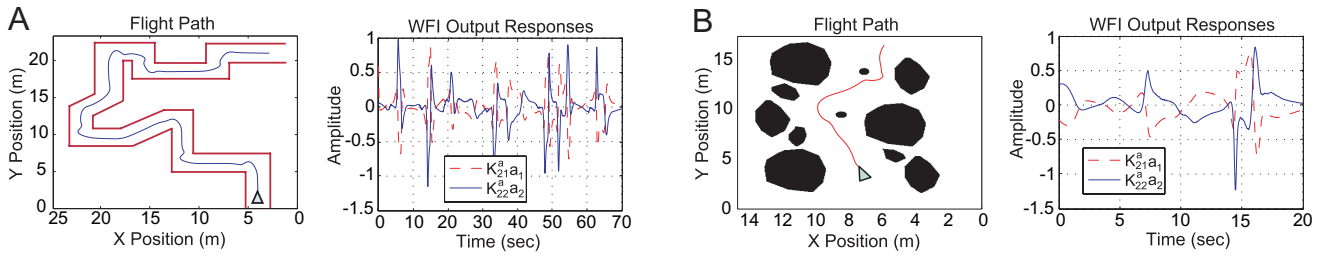

Fig. 6. Simulations of WFI-based navigation. (A) Corridor navigation (B) Obstacle field navigation navigation

Hence $u_2 = \langle \dot{Q}, F_{u_2} \rangle_w$, corresponding to the motion sensitivity function

$$F_{u_2}(\gamma) \quad = \quad K^a_{20} + K^a_{21} \cos\gamma + K^a_{22} \cos 2\gamma. \qquad (25)$$

With this choice of torque control, the characteristic equation for the linearized closed loop dynamics is

$$s^3 + \frac{K^a_{20}}{J} s^2 - \frac{8K^a_{21} v_0}{3J\pi a} s + \frac{v_0(K^a_{22} - \sqrt{2}K^a_{20})}{Ja^2} = 0. \qquad (26)$$

The natural dynamics contain only inertial and viscous terms; therefore to achieve a stable centering/obstacle avoidance response, we require $K^a_{21} < 0$ for rotational stiffness and $K^a_{22} > 0$ for lateral stiffness. Additionally, rotational damping can be added with $K^a_{20} > 0$; however the linearization of the DC component a_0 of $\dot{Q}$ also has a lateral imbalance term (20), and hence we further need the restriction $K^a_{22} > \sqrt{2}K^a_{20}$ to provide the correctly signed lateral stiffness required for a stable centering response.

B. Simulation Results

Simulations were constructed based on the full nonlinear planar flight dynamics (18) to study the performance of the proposed WFI-based control methodology in general environments composed of obstacles. Environments were defined as bitmaps, and the instantaneous optic flow was computed by estimating the depth at the current position and orientation at 60 equally-spaced circumferential points and combining it with the current kinematics according to (11). WFI outputs are generated at each time instant by taking the discrete inner product of the instantaneous optic flow with weighting functions corresponding to (22) and (25). The WFI output gains used in the simulation were chosen based on the the performance index of maximizing the bandwidth of the slow (lateral) mode in the linearized closed loop system (26). The vehicle was directed to navigate a complicated corridor (Figure 6A) and an obstacle field (Figure 6B). The response of the first two cosine harmonics of the optic flow are shown.

V. Conclusions

A control-oriented analytical model for spatial wide-field integration (WFI) of retinal image flow was developed. The model provides a unique characterization of information available for feedback from WFI sensory systems, and establishes the connection between global structure of optic flow (retinal motion sensitivity patterns) and the control-relevant information available for feedback.

The analysis presented suggests a more general functional role for wide-field sensitive neurons in navigation and flight control as well as a novel methodology for utilizing optic flow in bio-inspired applications. Through the LPTC-inspired wide-field integration approach developed in this paper, additional information is available from optic flow that can be used to significantly increase closed loop stability and performance, as well as simplify sensory and actuation requirements. Specifically, the lateral imbalance can be directly estimated from a $F(\gamma) = \cos 2\gamma$ motion sensitivity function, which eliminates the need for actively removing the rotation term from the DC component and allows for the possibility of injecting rotational damping using the $F(\gamma) = 1/\sqrt{2}$ motion sensitivity function. In addition, the orientation with respect to a balanced nearness function can be determined using a $F(\gamma) = \cos\gamma$ sensitivity, which can be used to add rotational stiffness to the loop, and the global translational image velocity can be extracted using the $F(\gamma) = \sin\gamma$ sensitivity, which can be used in forward speed regulation.

References

[1] M. Egelhaaf and A. Borst, "Motion computation and visual orientation in flies," *Comp. Biochem. Phisiol.*, vol. 104A, pp. 659–673, 1993.

[2] A. Borst and J. Haag, "Neural networks in the cockpit of the fly," *J. Comp. Physiol. A*, vol. 188, pp. 419–437, 2002.

[3] M. Frye and M. Dickinson, "Fly flight: A model for the neural control of complex behavior," *Neuron*, vol. 32, pp. 385–388, 2001.

[4] J. Gibson, *The perception of the visual world*. Boston: Houghton Mifflin, 1950.

[5] R. Wehner, "Matched filters – neuronal models of the external world," *J. Comp. Physiol. A*, vol. 161, pp. 511–531, 1987.

[6] M. Reiser, J. Humbert, M. Dunlop, D. D. Vecchio, R. Murray, and M. Dickinson, "Vision as a compensatory mechanism for disturbance rejection in upwind flight," in *Proceedings of the American Control Conference*, Boston, MA, 2004.

[7] H. Krapp, B. Hengstenberg, and R. Hengstenberg, "Dendritic structure and receptive-field organization of optic flow processing interneurons in the fly," *J. Neurophysiol.*, vol. 79, pp. 1902–1917, 1998.

[8] K. Hausen, "Motion sensitive interneurons in the optomotor system of the fly, part ii. the horizontal cells: Receptive field organization and response characteristics," *Biol. Cybern.*, vol. 46, pp. 67–79, 1982.

[9] H. Krapp and R. Hengstenberg, "Estimation of self-motion by optic flow processing in single visual interneurons," *Letters to Nature*, vol. 384, pp. 463–466, 1996.

[10] J. Koenderink and A. van Doorn, "Facts on optic flow," *Biol. Cybern.*, vol. 56, pp. 247–254, 1997.